ADVANCED MATERIALS INTERFACES
www.advmatinterfaces.de

Mussel Byssus Inspired Ionic Skin with Damage-Resistant Signal for Human–Machine Interaction

*Wenkai Wang, Huaiyu Song, Zekang Lu, Qing Zeng, Qinghao Wang, Cheng Ma, Hongjun Jin, Jinwan Qi, Tongyue Wu, Shuitao Gao, Mingning Zhu, Dongdong Lu, Jianbin Huang, and Yun Yan**

Reliable human–machine interactions rely highly on a material that can provide stable real-time conductivity in the presence of unexpected damage. The closest step toward this goal is to create various self-healing materials, but the performance of the material will inevitably be interrupted during the process of healing. Herein, it is reported that damage-resistant conductivity of a skin-like polyelectrolyte film electrode can be achieved by creating hierarchical pores in analogy to those in mussel byssus. The hierarchical porous structure in mussel byssus is well-known to expel water quickly from the rock surface, but its role in recovering the ionic conductivity has been overlooked. It is shown that the ionic conductivity in the porous film remains stable as long as a small part of the film is still in contacting, owing to the fast ion transportation in the hierarchical pores. As such, the real-time conductivity does not change even if the skin-like film is cut with a knife or pieced with a needle during work. It is envisioned that the current damage-resistant ionic electrode wants to open a new vista in the design of soft conductive devices for reliable human–machine interactions.

1. Introduction

Human–machine interaction is emerging as a promising technique in diversified fields ranging from wearable electronics and health care, to soft robotics.[1] Flexible skin-like electrodes capable of transducing the physical strains of skin into distinct electrical signals are of critical importance for effective human–machine interactions. An ideal skin-like electrode for this purpose should be able to provide a reliable electrical current for any subtle variation of physical strains. To this goal, people have exerted considerable efforts to create various flexible conductive soft materials with desired mechanical properties,[2] healability,[3] and adhesivity.[4] In particular, the healability of an adhesive soft material is of paramount importance in providing a reliable signal in repeated and long-term services. So far, diversified healable materials are produced as flexible skin-like electrodes.[5] However, it usually takes a considerable period for the material to recover its original conductive ability.[6] This inevitably causes a break in real-time measurement or a fake sensing signal. So far, damage-resistant skin-like electrodes that always provide continuous stable signals with excellent sensitivity in the presence of damage are still not available.

Proper adhesivity is another desired feature for the skin-like electrode since appropriate adhesiveness allows accurate capture of tiny muscle strains. To date, most adhesive materials are inspired by mussel byssus, which are well-known to play important roles in fixing mussels on rocks, reefs, or other hard surfaces. The strong interaction between the dopa units in the byssal protein and the solid surfaces is considered very critical

W. Wang, H. Song, Z. Lu, Q. Zeng, C. Ma, H. Jin, J. Qi, T. Wu, S. Gao, J. Huang, Y. Yan
Beijing National Laboratory for Molecular Sciences (BNLMS)
College of Chemistry and Molecular Engineering
Peking University
Beijing 100871, China
E-mail: yunyan@pku.edu.cn

Q. Wang
State Key Laboratory of Turbulence and Complex Systems
Intelligent Biomimetic Design Lab
College of Engineering
Peking University
Beijing 100871, China

M. Zhu
Department of Biomedical Engineering
Southern University of Science and Technology
Shenzhen 518055, China

D. Lu
Department of Materials Science and Engineering
Southern University of Science and Technology
Shenzhen 518055, China

The ORCID identification number(s) for the author(s) of this article can be found under https://doi.org/10.1002/admi.202201367.

DOI: 10.1002/admi.202201367

in fixing the mussels. For this reason, tremendous adhesive materials are developed by incorporating the dopa unit into a polymer.[7] However, the hierarchical porous structure of the byssus has long been neglected in the design of artificial flexible adhesive materials. Noticeably, there are large pores of micrometers as well as small pores of nanometer scale in the mussel byssus. These pores are considered to be helpful in expelling water from the wet solid surface so that the interaction between the dopa unit and the solid surface would not be interfered with by the hydration layer.[8] Actually, studies have revealed that water transportation in nanoscaled channels, such as carbon nanotubes, is 3 to 5 orders faster than that predicted from conventional fluid-flow theory,[9] and Jiang et al. proposed the concept of quantum-confined superfluids to explain the ultrafast water or ion transportation in nanoscaled channels.[10] We, therefore, envision if such pores are created for the flexible skin-like ionic electrode, the fast ion transportation may maintain the conductivity before the damage heals completely, thus offering continuous stable conductivity even in the presence of damage. However, this scenario has not been verified.

Herein, we report the construction of a damage-resistant adhesive flexible skin-like ionic electrode by creating hierarchical pores similar to that of mussel byssus using the strategy of solid-phase molecular self-assembly (SPMSA) recently developed by us.[11] This strategy states that for a precipitate formed with a pair of oppositely charged polyelectrolyte and amphiphile, condensing the precipitate with mild mechanical pressure would facilitate the merging of the nanocluster of amphiphiles into large meso phases to reduce interface energy, which finally leads to macroscopic transparent supramolecular films. In this work, three polyelectrolytes were employed instead of a pair of oppositely charged polyelectrolyte and amphiphile, in order to introduce conductive ions and 3D nanoscale channels into the film. Because of the strong electrostatic interactions, the oppositely charged polyelectrolyte chains cannot pair properly before the immediate precipitation. As a result, counterions are always sequestered in the precipitates to balance the local osmotic pressure.[12] In the meanwhile, the hydrogen bonding between the polyelectrolytes may facilitate further interactions between the electrostatically interacted polyelectrolytes, thus offering nano-scaled networks in the film and balancing the elastic and viscous properties of the resultant film. With this design, the ionic conduction remains constant as long as there is still a small connection in the damaged film, which allows offering a stable real-time measuring signal albeit the presence of cuts and breaks. In this way, we for the first time demonstrated the possibility to create damage-resistant robust flexible skin-like electrodes for human–machine interaction.

2. Results and Discussion

2.1. Film Formation

Figure 1A shows the schematic illustration of the procedure leading to the damage-resistant ionic skin-like electrode. Upon mixing the aqueous solution of three individual polyelectrolytes, namely, the cationic poly-dimethyl diallyl ammonium chloride (PDDA), the anionic polyacrylamide (APAm), and sodium polyglutamic acid (SPG) to reach charge-balance, a "putty-like" precipitate was formed immediately (Figure S1A, Supporting Information). Upon loading the precipitate onto a noodle machine (Figure 1B) to exert a mild mechanical pressure of 0.1–1 MPa, this PDDA-APAm-SPG (PAS) precipitate was transformed into a transparent film, as illustrated in Figure S1, Supporting Information. When varying the molar ratio between APAm and SPG from 0:1 to 1:0, the resultant material changes from elastic to viscous (Figures S2–S5, Supporting Information). At the molar ratio of APAm: SPG of 3:1, the film displays both elastic and viscous properties and has the best mechanical strength, which was employed in the following for further study. FTIR measurements (Figure S6, Supporting Information) indicate that electrostatic interactions have occurred between the ammonium cations of PDDA and the carbonate anions from APAm and SPG. In

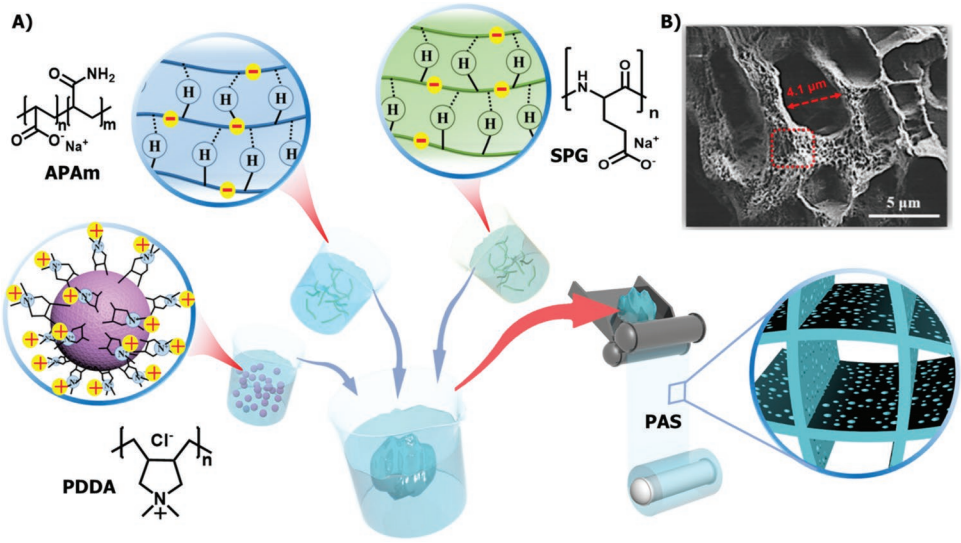

Figure 1. A) Illustration of the fabrication process of the ionic skin electrode PAS with three polyelectrolytes. B) The SEM image of the obtained PAS film electrode after freeze-drying.

the meanwhile, hydrogen bonding in the two anionic polymers of APAm and SPG occurs as well, which can be evidenced by the formation of network structures in their individual systems (Figure S7, Supporting Information). Elemental analysis confirms that besides the organic polymeric components, the resultant film contains 3.4% NaCl (Figure S8, Supporting Information). SEM examination reveals that there are hierarchical pores ranging from nanometers to micrometers in the film (Figure 1B), indicating the presence of sufficient 3D hierarchical channels for ion transportation.[13] Strikingly, these hierarchical pores are in high analogue to the microstructure of the natural byssus of mussels,[8a] which renders them the excellent adhesive ability to various surfaces (Figure S9, Supporting Information).

2.2. Mechanical Property

Because the component polyelectrolytes all have excellent hydration ability, the PAS film always contains a certain amount of water (Figure S10, Supporting Information). **Figure 2**A shows that as the water content varies from 5% to 55%, the fracture stress of the film decreases from ≈24.3 MPa to 80 KPa, while the maximum fracture strain increases from 5% to 1300%. It is noticed that Young's modulus of the PAS with 55% water is ≈40 kPa, which is similar to that of real human skin.[14] For this reason, the PAS containing 55 wt% water, recorded as PAS-55, is used as the skin-like electrode in this study.

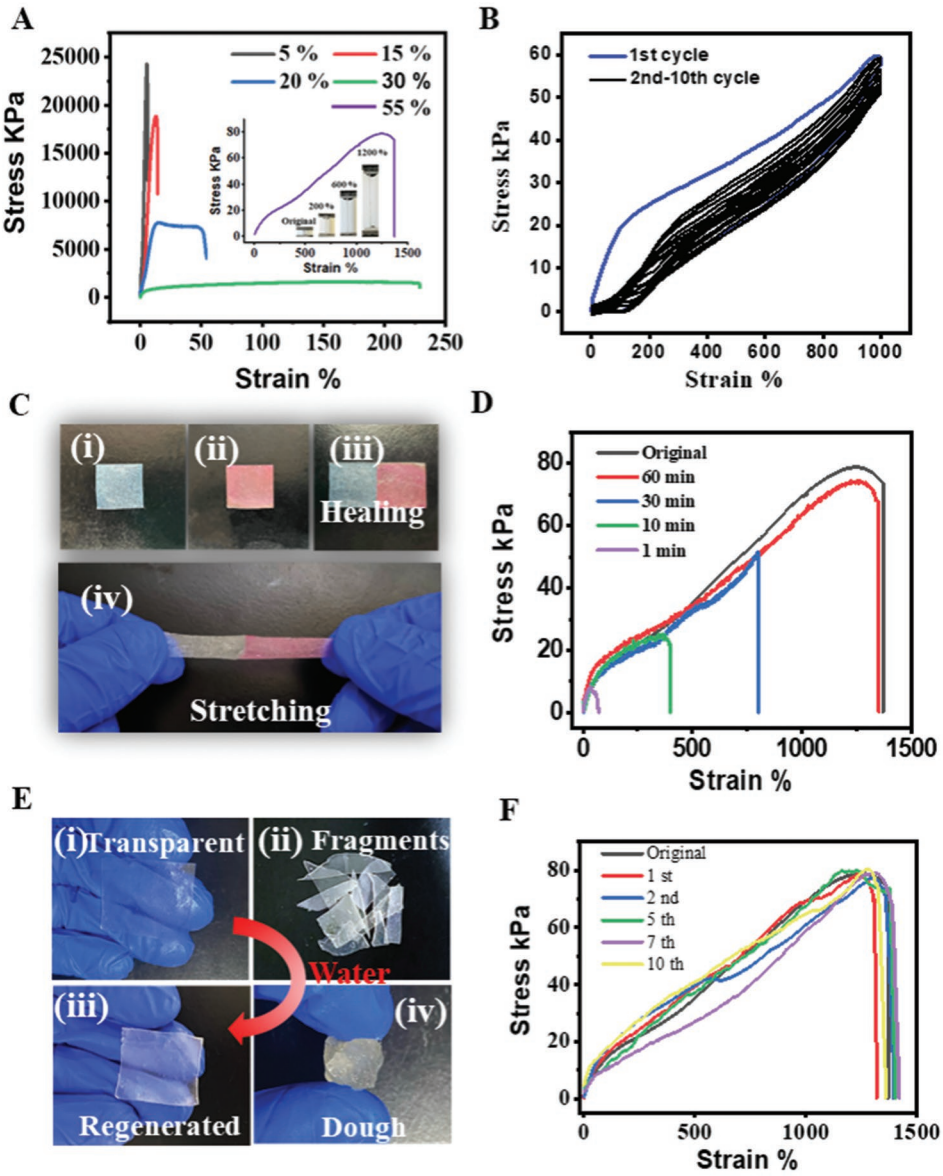

Figure 2. A) The tensile stress–strain tests of PAS with different contents of water. B) Ten successive loading-unloading cycles of PAS-55. C) Photo demonstration of the self-healing of two pieces of PAS dyed with Rhodamine 6G and methylene blue, respectively. D) The self-healing ability of the PAS in the time scale of 1, 10, 30, and 60 min under 100% humidity environment, respectively. E) The procedure used to regenerate the PAS. F) Stress–strain curves of the PAS films subjected to different numbers of cycles of remolding.

Figure 2B shows that the PAS-55 film displays excellent resilience. At a strain of 1000%, it exhibits a smaller hysteresis loop and a lower residual strain of 98% in the first loading-unloading cycle (blue line). The stress–strain curves in the subsequent nine loading–unloading cycles almost overlap with each other, indicating the PAS-55 is highly elastic and exhibits excellent resilience and fatigue resistance after the first loading–unloading cycle, which is qualified for the merit of "stretchability" desired in a damage-resistant film.

Figure 2C,D shows that the PAS-55 film is capable of instant self-healing. As two pieces of the PAS-55 films are brought to close contact, the two parts adhere together immediately. A stress of about 8 kPa has already been generated with a strain of about 30% within 1 min. The boundary disappears completely within 60 min, and 94.6% of the tensile stress and 98.6% of the strain is recovered (Figure 2D and Figure S11, Supporting Information). This excellent self-healing ability is attributed to the hydrogen bonding contributed by SPG, since solely electrostatic interaction between PDDA and APAm and the hydrogen bonding ability of APAm resulted in highly elastic materials (Figure S3A, Supporting Information) with microporous structure (Figure S3B, Supporting Information) which cannot repair themselves (Figure S4, Supporting Information), whereas the electrostatic interaction between PDDA and SPG merely leads to highly viscous fluid (Figure S5, Supporting Information). It is noticed that the self-healing ability also endows the film with satisfied recycling ability. If the film fragments are hydrated sufficiently with water (Figure 2E,F), a new film can be regenerated under mechanical pressure under ambient conditions. The mechanical strength of the regenerated film is the same as the original one (Figure 2F).

2.3. Adhesive Properties

Remarkably, the PAS-55 also displays excellent adhesive ability toward various surfaces, ranging from hydrophilic copper to the hydrophobic Teflon, and even wet biological tissues such as porcine (Figure S12, Supporting Information). The equilibrium adhesiveness to copper in 1 h is the strongest (Figure S13, Supporting Information), indicating it is very convenient to engineer an external circuit with a copper tip onto it. It is noticed that the adhesion to human skin is about 2.5 times better than commercial electrode hydrogels. The adhesion force of a PAS-55 film to the hairy skin is even stronger than to the naked one, which is evidenced by the 1.38 and 1.32 N cm^{-1} adhesion force for the former and latter, respectively (Figure S14A, Supporting Information). With this robust adhesive ability to skin, the PAS-55 can always co-shape with skin movement in the large range of convex and concave and gives corresponding positive and negative sensing signals (Figure S14B, Supporting Information). In particular, as the concave skin generates considerable wrinkles, the PAS-55 film can still adhere firmly (Figure S15A, Supporting Information), just like it is an intrinsic part of the skin. In contrast, the none-adhesive film would not co-shape with the concave skin actions and resulted in detaching (Figure S15B, Supporting Information). This much effective adhesion than the commercial electrode hydrogels does not bring up skin irritation and de-adhesion difficulties.[15] After being mounted on the skin of a volunteer for 2 h and then peeled off, the volunteer did not feel pain, and no film residue was left on the skin (Figure S16A, Supporting Information). Moreover, repeated adhesion is possible. The adhesiveness did not fatigue even after five cycles of deadhesion/adhesion (Figure S16B, Supporting Information). The 3-day culture of BSCL cells (Figure S17, Supporting Information) revealed that PAS has negligible cytotoxicity.

2.4. Damage-Resistant Conductivity

Since the film contains NaCl, the PAS-55 film displays an excellent conductivity of about 5.7 S m^{-1}, which is among the best ionic conductivities obtained so far (Figure S18 and Data S1, Supporting Information). Strikingly, the PAS-55 film displays amazing anti-fatigue and damage-resistant sensing ability. Most flexible electrodes rely on sufficient self-healing ability to provide reliable conductivity. Here we found the PAS-55 will always provide a reliable sensing signal even before complete self-healing. As cutting lines ranging from ≈1–4 cm were made with a knife in the film, the current recovered to the original value immediately as soon as the knife was removed (**Figure 3**A,B). Nearly no time delay at the level of second is detected for completed signal recovery. A similar stable current was observed as well as the completely separated films were brought to contact (Figure 3C). This is in clear contrast with most reported electrodes which undergo a sharp signal drop and only resume within hours.[16] Most interestingly, the current did not decrease noticeably even when the two separated parts are brought to contact vertically, although the contacting area is only about 1/10 of the damage. The photo in Figure 3C-ii shows that the LED is of the same light as the original one no matter whether the two separated parts are contacted vertically or horizontally, and the current remains basically the same in the three scenarios (Figure 3C-iii). In contrast, control experiments made with NaCl solutions showed a drastic current drop in reduced contact, which is also the case for other conductive films.[6a,c,11f] Figure 3D-i shows that as a channel bridge was set for two pools containing 3.4% NaCl solution, which is the same NaCl concentration as that in the PAS-55 film, the current is proportional to the width of the bridge. Clearly, the "partial healing" of a bulk water bridge would not lead to 100% conductivity recovery (Figure 3D-ii). This unambiguously manifests that the hierarchical pores in the PAS film are very crucial for the extremely fast propagation of the electric field, making the current film possible to serve as a damage-resistant strain sensor.

2.5. Damage-Resistant Ream-Time Human–Machine Interaction

The intrinsic ionic conductivity and excellent adhesive ability, in combination with the excellent mechanical properties, makes the PAS-55 an excellent skin-like electrode that can always provide stable electromyogram (EMG) signals in the presence of damage. **Figure 4**A shows as the PAS-55 film with a diameter of 2.0 cm was placed parallel on a volunteer's inner skin of the left forearm, and another PAS-55 film was attached to the elbow as

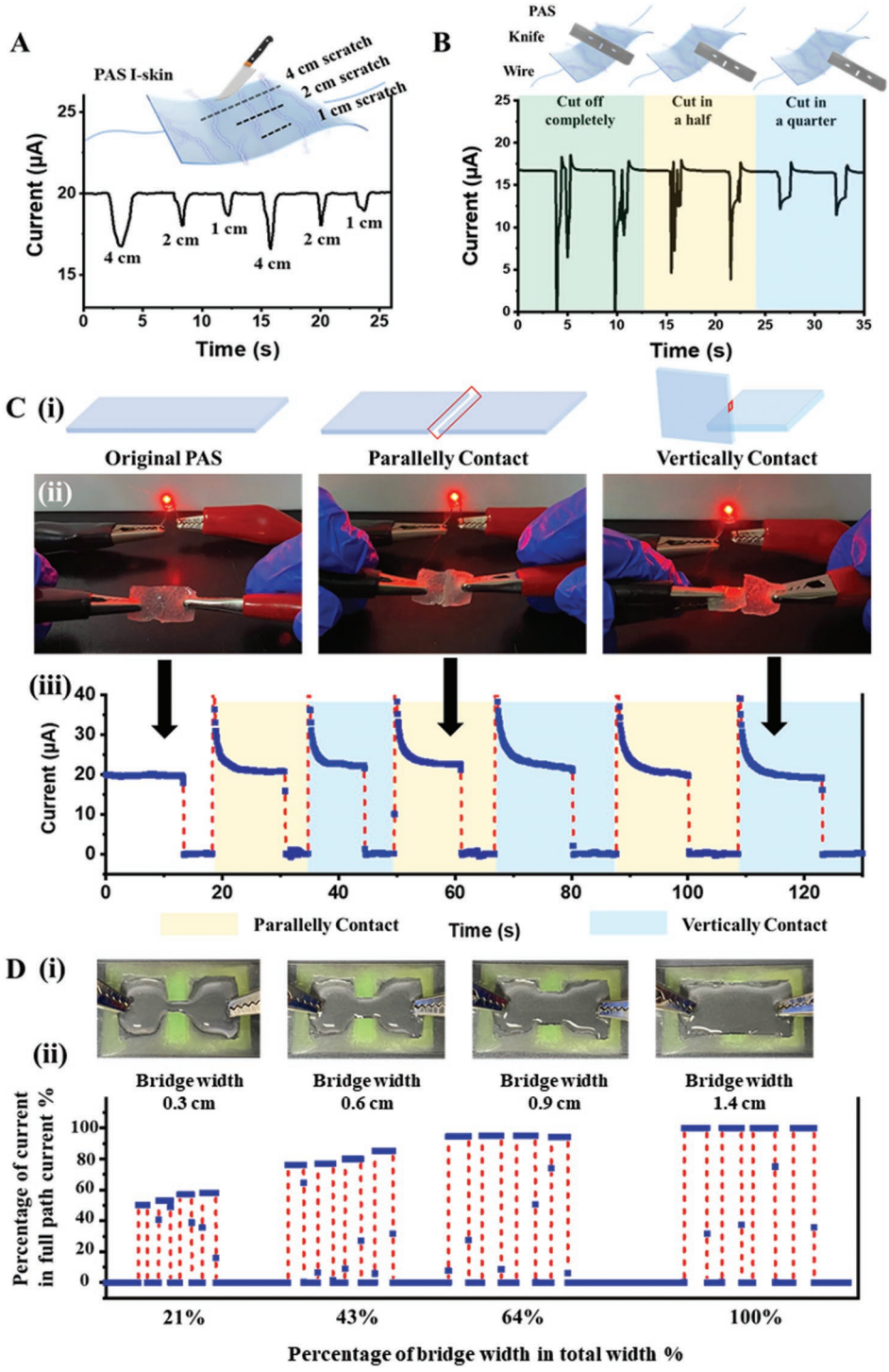

Figure 3. A) Real-time current changes of the blade scratching different lengths (1, 2, and 4 cm) on the PAS film surface in the parallel current direction, respectively. B) Real-time current changes of the blade scratching different lengths (a quarter width, half width, and completely) on the PAS film surface in the vertical current direction, respectively. C) i) The three different models of PAS film under the original state, parallelly contact and vertically contact, respectively; ii) the LED (0.05 W) was switched on instantly by the original PAS film and touching the two PAS films parallelly and vertically, respectively. iii) The Real-time current changes of the two PAS film contact parallelly and vertically, respectively. D) i) Salt bridge simulation experiment, photos of the salt bridge with different proportion width; ii) salt bridge simulation experiment, change the channel with different proportion width (0.3/1.4, 0.6/1.4, 0.9/1.4, and 1.4/1.4 cm), and the percentage of real-time current in the current of the complete channel.

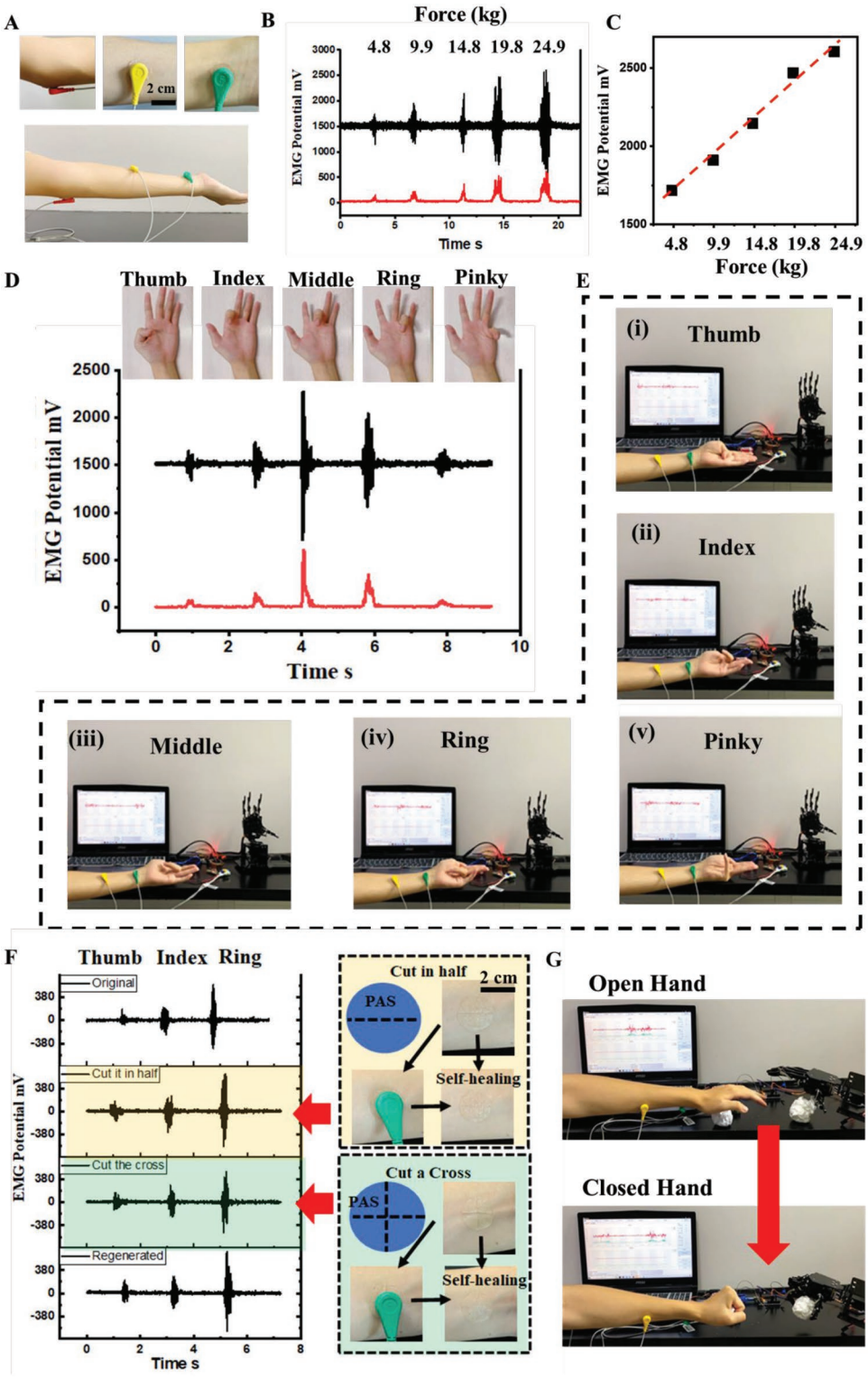

Figure 4. A) Digital photographs of the commercial digital converter and the EMG signal measurement using PAS. B) EMG signals acquired from the forearm with different grasping forces. C) Variations of the EMG signal amplitude and the gripping force. D) EMG signals produced by the flexion/extension of different fingers. E) Demonstration of an EMG recording and corresponding control of a robotic hand, showing five motions of five fingers and following motions of the robotic hand. F) EMG signals produced by the flexion/extension of different fingers before and after the PAS was cut, respectively. The self-healing occurs instantly after the cuts and the signal were recorded in real-time. G) Opening and closing movements of the hand through simple EMG signal recognition, and remotely controlling the robot hand to grasp objects.

the ground electrode, the detected EMG signal has a signal-to-noise ratio (SNR) of 44.5 dB, which is improved by over 60% compared with the 27.8 dB of the commercial electrode (Figure S19, Supporting Information). When the hand grips with forces of 4.8, 9.9, 14.8, 19.8, and 24.9 kg (Figure S20, Supporting Information), respectively, EMG signals proportional to the forces were obtained (Figure 4B,C). The sensitivity of EMG signals to muscle movement is so high that it can even differentiate the actions of a specific finger. Figure 4D shows as the PAS film was mounted on the arm, actions generated by different fingers give drastically different signals, and these delicate signals can be remotely recognized by the robot hand to yield exactly the same actions (Figure 4E and Movie S1, Supporting Information). This ultra-high sensibility is in clear contrast with the non-distinguishable EMG signals of specific fingers reported in other important works.[17] Strikingly, the PAS-55 electrode is able to offer damage-resistant sensitive real-time EMG signal even in the presence of cutting lines. As illustrated in Figure 4F, Movies S2 and S3, Supporting Information, no matter whether the PAS-55 film was cut into two parts or four parts, or pierced, the EMG signals of different fingers were not affected noticeably, verifying that it is indeed a damage-resistant skin-like electrode. With this excellent ability to collect EMG signals precisely, the robot hand is expected to conduct complicated actions commanded by a human. Figure 4G shows a simple demo of the PAS-55 electrode-enabled grasping (Movie S4, Supporting Information) and releasing objects with a robot hand. We envision the current work opens a new vista in the field of human–machine interaction materials.

3. Conclusion

In summary, we report it is possible to create a damage-resistant ionic skin-like electrode that always offers ultra-high real-time sensitivity in the presence of damage by mimicking the hierarchical porous structure of mussel byssus. This was achieved by carefully modulating the ionic and hydrogen bonding between three polyelectrolytes utilizing the strategy of solid phase molecular self-assembly (SPMSA). Since some small ions would always be arrested as the composite polyelectrolytes precipitate from water, the resultant film materials spontaneously possess ionic conductivity. The hierarchical porous structure in the film is nearly the same as that in the mussel byssus, which offers damage-resistance conductivity. We consider that the superior adhesiveness, satisfied flexibility, and instant self-healing ability chorus together to rebuild part of the porous structures, then the ultrafast transportation of water and ions in the nano-scaled channels leads to instant 100% recovery of the conductivity. We expect this work will update the design philosophy of advanced sensing materials and skin-like electrodes and offers a promising possibility for reliable human-machine interactions.

4. Experimental Section

Materials: Polydimethyl diallyl ammonium chloride PDDA (20 wt% in water, Mw = 400 000–500 000) was purchased from Shanghai Aladdin Biochemical Technology Co., Ltd. Sodium Poly-glutamic acid (SPG) (Mw = 50 000–150 000) was purchased from Heowns Co., Ltd. Anionic polyacrylamide (APAm) (Mw = 12 000 000) was purchased from Sangon Biotech (Shanghai) Co., Ltd. All these three polyelectrolytes were used directly without further purification. The commercial electrode hydrogels were polyurethane, acrylate elastomers, or silicone purchased from Wuxi Sizhirui Technology Co., Ltd.

Preparation of PAS I-Skin: Anionic polyacrylamide (APAm), sodium polyglutamic acid (SPG), and cationic poly-dimethyl diallyl ammonium chloride (PDDA) were purchased from Sigma-Aldrich Corporation. All other reagents were of AR grade. An aqueous solution of APAm and SPG, and an aqueous solution of PDDA were mixed, reaching final concentrations of 50 mM. White precipitates were immediately formed after the mixing and handshaking for 10 s. The collected precipitates were then subjected to a pressure imposed by finger pressing under ambient environment. The collected precipitates were then treated in two parallel ways: 1) subjected to a pressure imposed by finger pressing and became transparent after being preserved in a desiccator for 2.5 h or incubated in an oven at 60 °C for 0.5 h; and 2) in household noodle machine named Junxifu (Figure S1B, Supporting Information) manufacturing under ambient environment to exert a mild mechanical pressure of 0.1–1 MPa. The PAS was suspended in an atmosphere and equilibrated with different saturated salt solutions to obtain the different moisture content for 6 h, respectively. The relative humidity of the saturated salt solution is as follows: LiCl-11%, LiF-29%, NaBr-57%, NaCl-75%, and DI water-100%.

Mechanical Tests: The mechanical properties were tested by a tensile-testing machine (Instron 5943, TA) at room temperature. Stress–strain data were collected with a strain rate of 10 mm min^{-1}. All mechanical tests were conducted on dumbbell-shaped samples.

Adhesion Test: A sample for the peel test and lap shear adhesion test were prepared 8 × 8 mm. The peel test and lap shear adhesion test were conducted using an Instron 5943 machine at a pulling rate of 10 mm/min. The adhesion strength of the adhesive strain sensors was evaluated by both tests.

Ionic Conductivity Test: The voltage on the I-skin was controlled as constant at 1.0 V and monitored the current change when moved and talked. Then the electronic resistance variation ($\Delta R/R0$) could be calculated from the change of current.

Characterizations: Scanning electron microscopy (SEM) measurements were performed using a Hitachi S4800 microscope at an acceleration voltage of 1.0 kV. The films were placed on clean silicon wafers for SEM observations. All measurements were conducted using DI water at 20 °C. TGA experiments were carried out under nitrogen flow on TA Instrument Q600 SDT at a heating rate of 15 °C min^{-1}.

Cytotoxicity MTS Assays and Live/Dead Fluorescence Imaging: BSC1,[18] monkey kidney epithelial cells, were grown in Invitrogen α-minimum essential medium (α-MEM) with 5% fetal bovine serum (FBS) (Thermo-Fischer Scientific, USA), 1% sodium pyruvate (Gibco), 1% glutaMAXTM-1 (Gibco), and 1% penicillin-streptomycin (Thermo-Fischer Scientific, USA). The cells were maintained at 37 °C and humidified 5% CO_2 incubator. The toxicity of the PAS was evaluated to be similar to that previously reported.[19] A density of 5 × 103 BSC1 cells was seeded into a 24-well plate (Costar Corning Corp.,) in 1.5 mL and cultured for 1 day. On the following days, the cells with updated 1.5 mL α-MEM were exposed to 5 mm discs of gels (≈30–40 mg) for 1, 2, and 3 days. The gels were indirectly delivered to the adherent cells after being dispersed in α-MEM. Subsequently. A 40 ul MTS assay[20] (2 mg mL^{-1}) was performed to test the cytotoxicity of the hydrogels. As a positive control, the cells were just grown under α-MEM. Absorbance was measured at 490 nm after 1 h of incubation at 37 °C with a microplate reader (Synergy H1, Bio-Tek) for calculating the cell survival rates. Furthermore, a live/dead cell staining assay was performed to qualitatively evaluate and visualize cell viability after indirect contact with the coacervated PAS. The mass of PAS used for live/dead staining was similar to those used in the MTS studies.[20] The BSC1 cells (a density of 5 × 104) were seeded into a glass bottom dish (35 mm dish with 10 mm bottom well, Cellvis) and allowed to grow in α-MEM for 1 day. After that, the gels were indirectly exposed in the dish with updated 2 mL α-MEM for 1, 2, and 3 days. The cells were stained by live/dead assay. Live cells were stained with calcein AM as

green, whereas the dead cells were stained with ethidium homodimer-1 as the red color. For the positive control, BSC1 cells were incubated with pure α-MEM prior to the addition of the live/dead solution. Fluorescence images were obtained with a confocal laser scanning microscopy (LSM 900 with Airyscan).

Biopotential EMG Signal Extraction: The control system of robotic hands consisted of two parts, including sensitive electrodes and the signal processing setup. The EMG signals were acquired by two PAS film electrodes placed on the wrist flexors, as well as another PAS film electrode attached to the elbow as a reference electrode. The signals were generated by the action potential that occurs between working and reference electrodes during the contraction of the object muscular. The signal recording and processing setup include a microcontroller (Arduino UNO microcontroller) and a detector (EMG Sensor). The EMG electrodes detected the action potential of muscular contraction and outputted to Arduino UNO microcontroller, which performed signal processing algorithms (Root-Mean-Square, etc.) and identified the signals. The robotic hand then reproduced the same motion as the fingers according to the identification result.

Supporting Information

Supporting Information is available from the Wiley Online Library or from the author.

Acknowledgements

The authors thank Prof. Lei Jiang of the Science and Technology Institute, Chinese Academy of Science for the inspiring discussions, and thank Prof. Guangming Xie in State Key Laboratory of Turbulence and Complex Systems, Intelligent Biomimetic Design Lab, College of Engineering, Peking University for his valuable suggestions and technical assistance on manipulator. The authors also thank Prof. Changfeng Wu in Southern University of Science and Technology for their assistance and equipment support to cell experiments. This work was financially supported by the National Natural Science Foundation of China (NSFC 22172004, 21972003).

Conflict of Interest

The authors declare no conflict of interest.

Authors Contribution

W.W. and Y.Y. conceived the reaearch project and designed the experiments; W.W., H.S., Q.Z., and Q.W. completed the biopotential electromyogram signal extraction and robot hand experiments; W.W. and Z.L. prepared the materials and permofrmend the damage-resistant conductivity experimrnts; H.J., J.Q., T.W. and C.M. performed the TGA, ATR-IR, SEM, TEM, and mechanical tests; W.W. and S.G. performed the adhesion experiment; M.Z. and D.L. performed the Cytotoxicity MTS Assays and Live/Dead Fluorescence Imaging experiments; W.W., Y.Y., and J.H. contributed to analyzing the results; W.W. and Y.Y. wrote the manuscript; all the authors contributed to editing the manuscript. Y.Y. supervised the research.

Data Availability Statement

The data that support the findings of this study are available from the corresponding author upon reasonable request.

Keywords

conductivity, damage-resistant, hierarchical pores, ionic skin, mussel byssus

Received: June 18, 2022
Revised: August 30, 2022
Published online:

[1] a) C. Majidi, *Soft Rob.* **2014**, *1*, 5; b) M. Cianchetti, C. Laschi, A. Menciassi, P. Dario, *Nat. Rev. Mater.* **2018**, *3*, 143; c) M. Zhu, Z. Sun, Z. Zhang, Q. Shi, T. He, H. Liu, T. Chen, C. Lee, *Sci. Adv.* **2020**, *6*, aaz8693; d) R. Yin, D. Wang, S. Zhao, Z. Lou, G. Shen, *Adv. Funct. Mater.* **2021**, *31*, 2008936; e) G.-H. Lee, H. Moon, H. Kim, G. H. Lee, W. Kwon, S. Yoo, D. Myung, S. H. Yun, Z. Bao, S. K. Hahn, *Nat. Rev. Mater.* **2020**, *5*, 149; f) I. You, D. G. Mackanic, N. Matsuhisa, J. Kang, J. Kwon, L. Beker, J. Mun, W. Suh, T. Y. Kim, J. B.-H. Tok, Z. Bao, U. Jeong, *Science* **2020**, *370*, 961; g) W. Wang, S. Wang, R. Rastak, Y. Ochiai, S. Niu, Y. Jiang, P. K. Arunachala, Y. Zheng, J. Xu, N. Matsuhisa, X. Yan, S.-K. Kwon, M. Miyakawa, Z. Zhang, R. Ning, A. M. Foudeh, Y. Yun, C. Linder, J. B. H. Tok, Z. Bao, *Nat. Electron.* **2021**, *4*, 143.

[2] a) T. Sekitani, Y. Noguchi, K. Hata, T. Fukushima, T. Aida, T. Someya, *Science* **2008**, *321*, 1468; b) T. Li, Y. Wang, S. Li, X. Liu, J. Sun, *Adv. Mater.* **2020**, *32*, 2002706; c) T. Long, Y. Li, X. Fang, J. Sun, *Adv. Funct. Mater.* **2018**, *28*, 1804416; d) J. Xu, H.-C. Wu, C. Zhu, A. Ehrlich, L. Shaw, M. Nikolka, S. Wang, F. Molina-Lopez, X. Gu, S. Luo, D. Zhou, Y.-H. Kim, G.-J. N. Wang, K. Gu, V. R. Feig, S. Chen, Y. Kim, T. Katsumata, Y.-Q. Zheng, H. Yan, J. W. Chung, J. Lopez, B. Murmann, Z. Bao, *Nat. Mater.* **2019**, *18*, 594.

[3] a) P. Cordier, F. Tournilhac, C. Soulie-Ziakovic, L. Leibler, *Nature* **2008**, *451*, 977; b) B. Ghosh, M. W. Urban, *Science* **2009**, *323*, 1458; c) M. Burnworth, L. M. Tang, J. R. Kumpfer, A. J. Duncan, F. L. Beyer, G. L. Fiore, S. J. Rowan, C. Weder, *Nature* **2011**, *472*, 334; d) Y. Yanagisawa, Y. Nan, K. Okuro, T. Aida, *Science* **2018**, *359*, 72; e) J. Kang, J. B. H. Tok, Z. Bao, *Nat. Electron.* **2019**, *2*, 144.

[4] a) C. Heinzmann, C. Weder, L. M. de Espinosa, *Chem. Soc. Rev.* **2016**, *45*, 342; b) S. Lamping, T. Otremba, B. J. Ravoo, *Angew. Chem., Int. Ed.* **2018**, *57*, 2474; c) Y. Xue, J. Zhang, X. Chen, J. Zhang, G. Chen, K. Zhang, J. Lin, C. Guo, J. Liu, *Adv. Funct. Mater.* **2021**, *31*, 2106446; d) J. Deng, H. Yuk, J. Wu, C. E. Varela, X. Chen, E. T. Roche, C. F. Guo, X. Zhao, *Nat. Mater.* **2021**, *20*, 229; e) H. Yuk, C. E. Varela, C. S. Nabzdyk, X. Mao, R. F. Padera, E. T. Roche, X. Zhao, *Nature* **2019**, *575*, 169.

[5] a) T. Q. Trung, N.-E. Lee, *Adv. Mater.* **2016**, *28*, 4338; b) J. C. Yang, J. Mun, S. Y. Kwon, S. Park, Z. Bao, S. Park, *Adv. Mater.* **2019**, *31*, 1904765; c) C. Shao, M. Wang, L. Meng, H. Chang, B. Wang, F. Xu, J. Yang, P. Wan, *Chem. Mater.* **2018**, *30*, 3110; d) L. M. Zhang, Y. He, S. Cheng, H. Sheng, K. Dai, W. J. Zheng, M. X. Wang, Z. S. Chen, Y. M. Chen, Z. Suo, *Small* **2019**, *15*, 1804651; e) Z. Xu, L. Chen, L. Lu, R. Du, W. Ma, Y. Cai, X. An, H. Wu, Q. Luo, Q. Xu, Q. Zhang, X. Jia, *Adv. Funct. Mater.* **2021**, *31*, 2006432.

[6] a) Y.-J. Liu, W.-T. Cao, M.-G. Ma, P. Wan, *ACS Appl. Mater. Interfaces* **2017**, *9*, 25559; b) B. Li, L. Kan, S. Zhang, Z. Liu, C. Li, W. Li, X. Zhang, H. Wei, N. Ma, *Nanoscale* **2019**, *11*, 467; c) C. Wang, X. Qu, Q. Zheng, Y. Liu, P. Tan, B. Shi, H. Ouyang, S. Chao, Y. Zou, C. Zhao, Z. Liu, Y. Li, Z. Li, *ACS Nano* **2021**, *15*, 10130.

[7] W. Zhang, R. Wang, Z. Sun, X. Zhu, Q. Zhao, T. Zhang, A. Cholewinski, F. Yang, B. Zhao, R. Pinnaratip, P. K. Forooshani, B. P. Lee, *Chem. Soc. Rev.* **2020**, *49*, 433.

[8] a) B. P. Lee, P. B. Messersmith, J. N. Israelachvili, J. H. Waite, *Annu. Rev. Mater. Res.* **2011**, *41*, 99; b) T. Priemel, G. Palia, F. Förste,

F. Jehle, S. Sviben, I. Mantouvalou, P. Zaslansky, L. Bertinetti, M. J. Harrington, *Science* **2021**, *374*, 206.

[9] a) M. Majumder, N. Chopra, R. Andrews, B. J. Hinds, *Nature* **2005**, *438*, 930; b) J. K. Holt, H. G. Park, Y. M. Wang, M. Stadermann, A. B. Artyukhin, C. P. Grigoropoulos, A. Noy, O. Bakajin, *Science* **2006**, *312*, 1034.

[10] L. P. Wen, X. Q. Zhang, Y. Tian, L. Jiang, *Sci. China Mater.* **2018**, *61*, 1027.

[11] a) M. Xie, Y. Che, K. Liu, L. Jiang, L. Xu, R. Xue, M. Drechsler, J. Huang, B. Z. Tang, Y. Yan, *Adv. Funct. Mater.* **2018**, *28*, 1803370; b) H. Jin, M. Xie, W. Wang, L. Jiang, W. Chang, Y. Sun, L. Xu, S. Zang, J. Huang, Y. Yan, *CCS Chem.* **2020**, *2*, 98; c) W. Wang, M. Xie, H. Jin, W. Zhi, K. Liu, C. Ma, P. Liao, J. Huang, Y. Yan, *Mater. Chem. Front.* **2020**, *4*, 1530; d) H. Jin, C. Ma, W. Wang, Y. Cai, J. Qi, T. Wu, P. Liao, H. Li, Q. Zeng, M. Xie, *ACS Mater. Lett.* **2021**, *4*, 145; e) P. Liao, S. Zang, T. Wu, H. Jin, W. Wang, J. Huang, B. Z. Tang, Y. Yan, *Nat. Commun.* **2021**, *12*, 5496; f) T. Wu, S. Gao, W. Wang, J. Huang, Y. Yan, *ACS Appl. Mater. Interfaces* **2021**, *13*, 41997; g) S. Gao, J. Qi, S. Jiang, T. Wu, W. Wang, Y. Cai, C. Ma, B. Zhang, J. Huang, Y. Yan, *ACS Appl. Bio Mater.* **2021**, *4*, 7314; h) S. Gao, W. Wang, T. Wu, S. Jiang, J. Qi, Z. Zhu, B. Zhang, J. Huang, Y. Yan, *ACS Appl. Mater. Interfaces* **2021**, *13*, 34843; i) J. Qi, T. Wu, W. Wang, H. Jin, S. Gao, S. Jiang, J. Huang, Y. Yan, *Aggregate* **2022**, *3*, 173.

[12] a) C. H. Porcel, J B. Schlenoff, *Biomacromolecules* **2009**, *10*, 2968; b) H. H. Hariri, J. B. Schlenoff, *Macromolecules* **2010**, *43*, 8656; c) A. Reisch, P. Tirado, E. Roger, F. Boulmedais, D. Collin, J. C. Voegel, B. Frisch, P. Schaaf, J. B. Schlenoff, *Adv. Funct. Mater.* **2013**, *23*, 673.

[13] Y. Zhou, C. Wan, Y. Yang, H. Yang, S. Wang, Z. Dai, K. Ji, H. Jiang, X. Chen, Y. Long, *Adv. Funct. Mater.* **2019**, *29*, 1806220.

[14] Y. Yu, H. Yuk, G. A. Parada, Y. Wu, X. Liu, C. S. Nabzdyk, K. Youcef-Toumi, J. Zang, X. Zhao, *Adv. Mater.* **2019**, *31*, 1807101.

[15] A. Miyamoto, S. Lee, N. F. Cooray, S. Lee, M. Mori, N. Matsuhisa, H. Jin, L. Yoda, T. Yokota, A. Itoh, M. Sekino, H. Kawasaki, T. Ebihara, M. Amagai, T. Someya, *Nat. Nanotechnol.* **2017**, *12*, 907.

[16] a) T. Li, Y. Wang, S. Li, X. Liu, J. Sun, *Adv. Mater.* **2020**, *32*, 2002706; b) S. Li, H. Pan, Y. Wang, J. Sun, *J. Mater. Chem. A* **2020**, *8*, 3667.

[17] a) L. Zhang, K. S. Kumar, H. He, C. J. Cai, X. He, H. Gao, S. Yue, C. Li, R. C.-S. Seet, H. Ren, J. Ouyang, *Nat. Commun.* **2020**, *11*, 4683; b) Y. Zhao, S. Zhang, T. Yu, Y. Zhang, G. Ye, H. Cui, C. He, W. Jiang, Y. Zhai, C. Lu, X. Gu, N. Liu, *Nat. Commun.* **2021**, *12*, 4880; c) S. Zheng, W. Li, Y. Ren, Z. Liu, X. Zou, Y. Hu, J. Guo, Z. Sun, F. Yan, *Adv. Mater.* **2022**, *34*, 2106570.

[18] B. C. Goess, R. N. Hannoush, L. K. Chan, T. Kirchhausen, M. D. Shair, *J. Am. Chem. Soc.* **2006**, *128*, 5391.

[19] D. Lu, M. Zhu, S. Wu, Q. Lian, W. Wang, D. Adlam, J. A. Hoyland, B. R. Saunders, *Adv. Funct. Mater.* **2020**, *30*, 1909359.

[20] S. Basu, S. Pacelli, Y. Feng, Q. Lu, J. Wang, A. Paul, *ACS Nano* **2018**, *12*, 9866.